

Enhanced electrocaloric effect in compositional driven potassium sodium niobate-based relaxor ferroelectrics

Nan Zhang, Ting Zheng, Chunlin Zhao, Xiaowei Wei, Jiagang Wu^{a)}

Department of Materials Science, Sichuan University, Chengdu 610065, China

^{a)}Address all correspondence to this author. e-mail: wujiagang0208@163.com

Received: 20 August 2020; accepted: 22 September 2020; published online: 22 February 2021

Lead-free ferroelectric electrocaloric ceramics that could convert electrical energy into heat are the promising candidate for environment-friendly cooling devices. For refrigeration devices, a large temperature change (ΔT) and good temperature stability are required, which are highly related to the phase structure and the applied electric field. In this work, a diffused ferroelectric–paraelectric (FP) phase transition is formed in (K, Na)NbO₃ (KNN) by using appropriate composition engineering. The relaxor ferroelectrics in this work present both a large ΔT of 1.24 K and a high $\Delta T/\Delta E$ of 0.19 K mm/kV. In addition, a wide temperature span exceeds 55 °C at the high electrocaloric effect (ECE) criterion ($\Delta T \geq 0.5$ K) could also be observed. This work not only opens a new strategy for obtaining high-performance ceramics for refrigeration devices but also extends the application area of the KNN-based lead-free ferroelectrics from sensors, actuators and energy harvesting to solid-state cooling applications.

Introduction

Electrocaloric effect (ECE) is the ability to convert electrical energy to heat and *vice versa* of polar materials, which is consisted with the adiabatic temperature change (ΔT) and the isothermal entropy change (ΔS) under the process of applying and removing the external electric fields [1, 2, 3, 4]. As shown in Fig. 1(a), the large polarization change (ΔP) induced from the process of transforming disordered dipole moments to ordered one under the external electric field could lead to a high ΔT value. Since the giant ECE ($\Delta T_{\max} = 12$ K) observed in PZT thin films, multitudinous investigations have been conducted in the last few decades [5]. Although large ΔT (10–40 K) values could be found in thin films and polymers because of their high breakdown electric field strength, the bulk materials with high heating or cooling capacity are more suitable for medium-sized cooling applications [6]. Additionally, lead-free-based materials with large ECE have attracted much attention due to the environmental-friendly nature since the lead-based materials have a large amount of Pb and are harmful to human health and environment as well [7, 8]. Among the lead-free ceramics, (K, Na)NbO₃ (KNN)-based ceramics are one of the noted family of lead-free ferroelectric materials, and lots of researches have been conducted to improve

piezoelectric and ferroelectric properties by constructing phase boundary or domain structures [9, 10]. And some works have also been down to investigate the ECE performance in KNN-based ceramics around the phase boundary due to the furious polarization change under the external electric fields [7, 11]. For example, a ΔT value of 0.51 K is presented at ferroelectric–ferroelectric (FF) phase transition under 40 kV/cm [12]. A higher electrocaloric response of 1.19 K could be attained at ferroelectric–paraelectric (FP) phase boundary under 35 kV/cm [13]. And a larger ΔT value of 0.63 and 1.9 K could be observed under 80 and 159 kV/cm at around FF and FP, respectively [7, 14]. As a result, both the FP phase transition and the large applied electric field are beneficial for obtaining high ΔT values [6].

Generally, according to the temperature-dependent dielectric permittivity, KNN-based ceramic undergoes cubic (C)–tetragonal (T)–orthorhombic (O)–rhombohedral (R) phase transformations when testing temperature changes from high to low, and the temperature of C–T or FP phase transition can be tuned toward room temperature by doping ions like Sb⁵⁺, Ta⁵⁺, Ca²⁺, *etc.* [15]. As presented in Fig. 1(b), diffused FP phase transition at around room temperature in KNN-based ceramics can be formed by doping high content

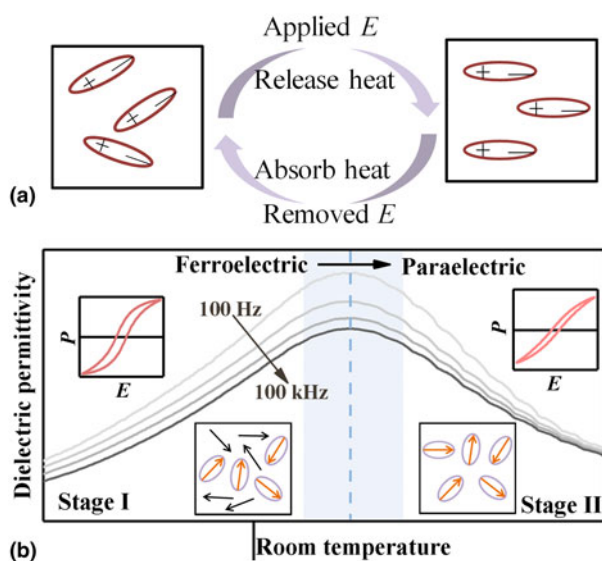


Figure 1: (a) Schematic of electrocaloric cooling cycle when applying and removing the external electric fields for polar materials. (b) Temperature-dependent dielectric permittivity measured at 0.1, 1, 10, and 100 kHz: the upper inset polarization hysteresis (P - E) loops are measured at the temperature below (Stage I) and above (Stage II) T_C , and the lower inset presents the schematic domain configurations of Stage I and Stage II, respectively.

ions, and two stages can be found in the dielectric curves [16, 17]. KNN-based relaxor ferroelectrics in Stage I possess a broad distribution size of nano-sized domains and a certain volume fraction of polar nanoregions (PNRs) when the temperature of the maximum dielectric constant gradually shifts to around room temperature, where the long-range-ordered matrix is destroyed owing to the high amount of chemical doping. Subsequently, with the further increased temperature, relaxor ferroelectrics reach Stage II with only PNRs existing in the non-polar matrix [18]. Consequently, typical P - E loop could be observed in Stage I, while a slimmer P - E loop with a degenerated polarization property is observed in Stage II. And a large polarization change (ΔP) value would be observed in the process of the transition between the typical P - E loop to slim P - E loop when the temperature increases and passes the FP phase transition. The ECE values of the ceramics could be calculated through the indirect method using the Maxwell relation:

$$\Delta T = -\frac{T}{\rho} \int_{E_1}^{E_2} \frac{1}{C_p} \left(\frac{\partial P}{\partial T} \right)_E dE, \quad (1)$$

where ρ is the density, C_p is the specific heat capacity per mass, T is the testing temperature, P is the ferroelectric polarization, E_1 and E_2 are the initial and final external electric fields, respectively [19, 20, 21]. For ferroelectrics, when the FP phase transition occurred with the elevated temperature, Eq. (1) could

be adapted utilizing the Curie-Weiss law:

$$\Delta T = \frac{\epsilon_0 C T}{2\rho C_p (T - T_C)^2} \Delta E^2 = \frac{T}{2\epsilon_0 C_p C_p} \Delta P^2, \quad (2)$$

where ϵ_0 is the dielectric permittivity of a vacuum and C is the Curie constant [22]. Apparently, the ΔT value is proportional to the square of electric field or the polarization. As a consequence, the high dielectric strength (high breakdown electric field), which could against high electric field, is favorable for obtaining high ΔT value. Besides, with the increasing temperature, a large ΔT value could be obtained near the T_C peak due to the generated large ΔP value caused by the high electric polarization and weakly inter-coupled domains, as well as the diffused FP phase transition [23].

In this work, Sb^{5+} is selected as the dopant atom in the KNN-based matrix to decrease the T_C and form a diffused FP phase transition at around room temperature. A large ΔT value could be obtained due to the produced large ΔP when the testing temperature increases and passes the FP transition. In addition, CuO is introduced into the KNN-based matrix to facilitate the sintering process and improve the breakdown electric field strength, which could influence the magnitude of ECE. Finally, large ΔT and $\Delta T/\Delta E$ of 1.24 K and 0.19 K mm/kV are obtained, and the temperature span at the high ECE norm ($\Delta T \geq 0.5$ K) could exceed 55 °C. In addition, both indirect and direct measurements are conducted to evaluate the veracity and magnitude of the calculated ECE properties. The high ECE value and a wide range of temperature span in this work indicate that the ceramics prepared in this study are hopeful materials for practical cooling applications.

Results and Discussion

Figures 2(a) and 2(b) show the room temperature X-ray diffraction (XRD) results and the enlarged XRD patterns around 32° (110) and 45° (200) of the ceramics with $x = 0.08 - 0.15$, respectively. All samples show perovskite structures, but a minor secondary phase could be observed when $x > 0.08$, which might be consist of $K_4CuNb_8O_{23}$ [24, 25]. In general, Cu^{2+} ion is considered to enter the B-site of the KNN unit cell and replace the Nb^{5+} ion because of the similar radius of Cu^{2+} (~73 pm) with Nb^{5+} (~64 pm) [26]. As reported, it is possible that a $K_4CuNb_8O_{23}$ liquid phase should be formed around 1050 °C due to the lower eutectic point of ~1020 °C between Nb_2O_5 and CuO [27]. As a consequence, with the increased Sb^{5+} substituting Nb^{5+} , considering the limited solubility in the B-sites of the KNN matrix, the replaced Nb^{5+} ions and the volatilized alkalis elements as well as the doped Cu^{2+} ions might form $K_4CuNb_8O_{23}$ liquid phase at the sintering temperature range of 1060–1080 °C and existed as a secondary phase in the perovskite. In addition, it can be seen that all

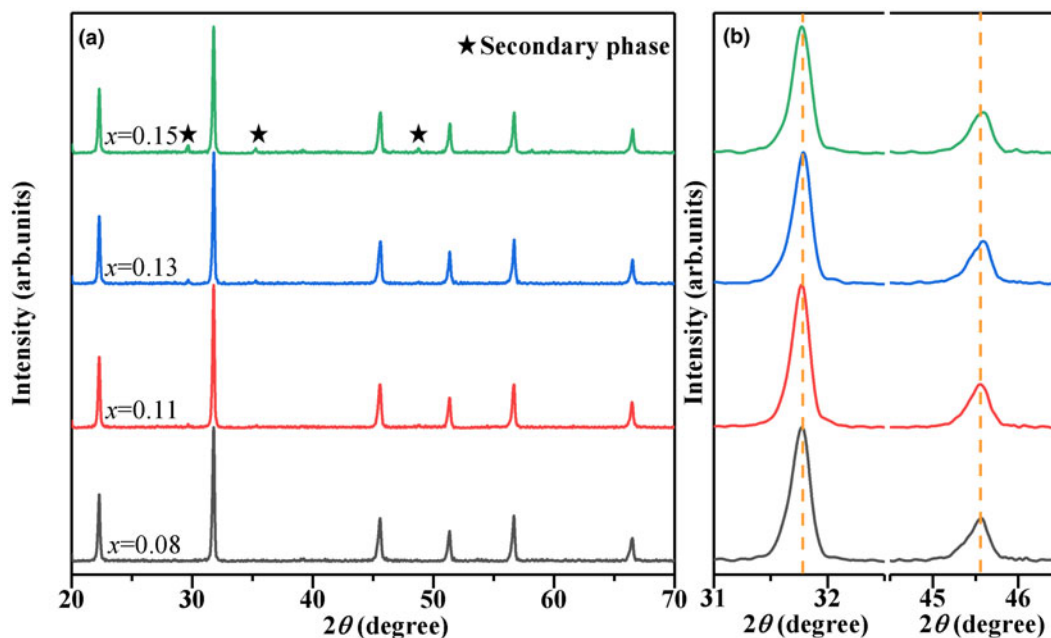


Figure 2: (a) Room temperature XRD patterns and (b) enlarged XRD patterns around 32° and 45° of the ceramics.

ceramics present the pseudo-cubic phase structure because no peak splitting could be observed in the peaks of (110) and (200), as shown in Fig. 2(b). Moreover, the (110) and (200) peaks shifts to a higher angle with increasing x content to 0.13, illustrating that the smaller radii ion Sb^{5+} (60 pm) enters the B-site of the KNN matrix and takes the place of Nb^{5+} (64 pm) [28]. With the further increased x content, the (110) peak shifts to a lower angle, which might be because of the limitation of solubility in the B-sites resulting in the more content of the secondary phase.

Figure 3(a) shows the temperature-dependent dielectric constant curves of the ceramics with $x = 0.08\text{--}0.15$ measured at 1, 10, and 100 kHz. The temperature of the maximum value of the dielectric constant (T_m , $\sim T_C$) decreases when x increases from 0.08 to 0.15, indicating that the increased Sb^{5+} substituting Nb^{5+} content could decrease T_C toward room temperature, as previously reported [15, 29]. Furthermore, for the all ceramics, the T_m value shifts to a higher temperature, while the maximum value of the dielectric constant at T_m decreases with the increased frequencies, indicating that the samples are relaxor ferroelectrics. Afterwards, more characterizations are conducted to further investigate the relaxation degree of the ceramics, as shown in Figs. 3(b) and 3(c). Figure 3(b) shows the $1/\epsilon_r\text{--}T$ curves of the ceramics with $x = 0.08\text{--}0.15$, respectively. A distinct divergence from the Curie–Weiss law could be observed, which can be described by the parameter of

$$\Delta T_m = T_{CW} - T_m, \quad (3)$$

where T_{CW} is the temperature at which dielectric permittivity begins to deviate the Curie–Weiss law and T_m represents the temperature at which the dielectric permittivity is the maximum value measured at 100 kHz [30]. As shown in Fig. 3(c), the diffuseness of the FP phase transition can be denoted by the modified Curie–Weiss law of

$$\frac{1}{\epsilon_r} - \frac{1}{\epsilon_m} = \frac{(T - T_m)^\gamma}{C}, \quad (4)$$

where ϵ_m is the maximum dielectric permittivity value, γ is the degree of diffuseness, and C is the Curie–Weiss constant [31]. In general, $\gamma = 1$ represents typical ferroelectrics, while $\gamma = 2$ describes ideal relaxor ferroelectrics undergoing diffuse phase transition [32]. The slope of the fitting data represents the magnitude of γ value, as shown in the inset of Fig. 3(c). As shown in Fig. 3(d), the similar variation of γ and ΔT_m values could be observed, both increasing quickly for $x \leq 0.11$ and then elevating slowly with the further increased x content. It means that the relaxation degree increases with the increased doping content, which is related to the decreased T_C values with the increased chemical substitution. In addition, the high γ values of >1.6 and ΔT_m values of >100 illustrate that a relatively high diffuseness of FP phase transition is obtained, which might be beneficial for a broad temperature span of ECE [23].

Figure 4 presents the temperature dependence of ferroelectric hysteresis ($P\text{--}E$) of the ceramics measured at 40 kV/cm. Typical $P\text{--}E$ loops could be observed in the ceramics with $x = 0.08\text{--}0.13$ with similar magnitude of P_{\max} , while a slimmer $P\text{--}E$ curve with rapidly deteriorated P_{\max} is present in $x =$

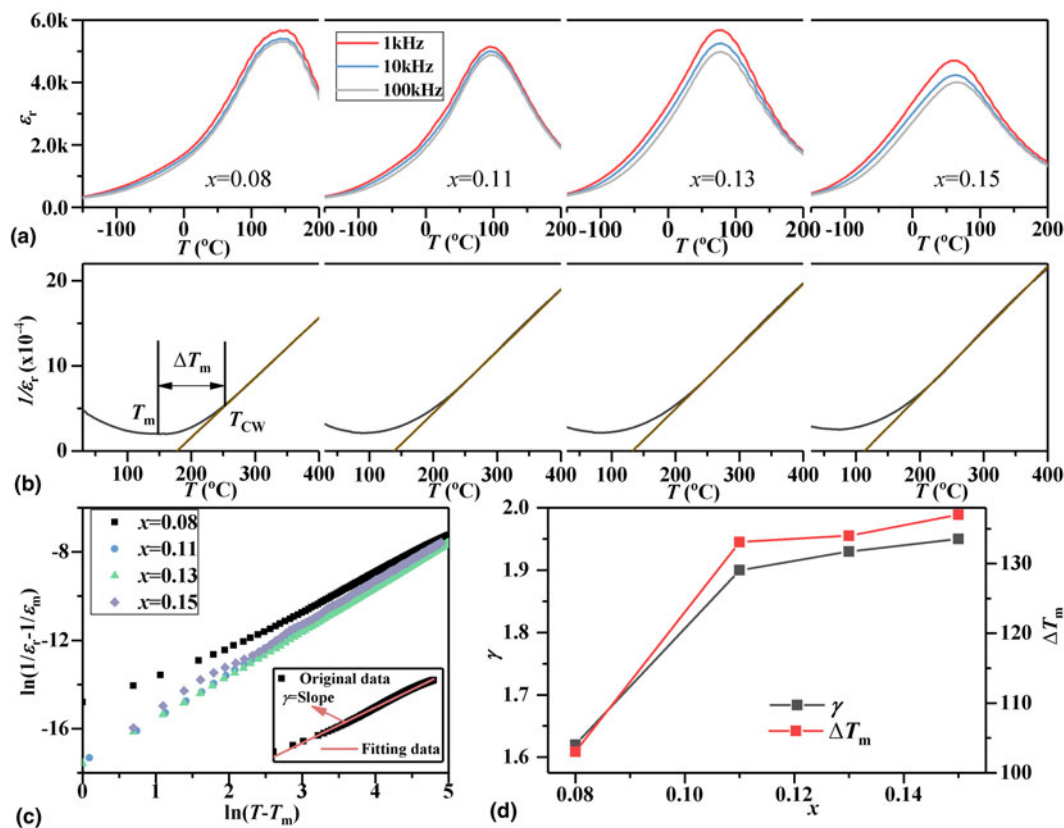


Figure 3: (a) Temperature-dependent ϵ_r curves measured at -150 – 200 °C and different frequencies of the ceramics; (b) $1/\epsilon_r$ – T curves measured at 30 – 400 °C and 100 kHz; (c) $\ln(1/\epsilon_r - 1/\epsilon_m) - \ln(T - T_m)$ curves of the ceramics measured at 100 kHz, the inset plot illustrate that the degree of diffuseness γ is fitted from the modified Curie–Weiss law; and (d) composition-dependent γ and ΔT_m of the ceramics.

0.15, illustrating that a degenerated polarization property is induced at $x = 0.15$, which may result in a deteriorated ECE performance. And the inset of Fig. 4 plots the P_{\max} – T curves under different electric fields. The P_{\max} values of the ceramics with $x = 0.08$ – 0.15 decrease with the increased temperature, illustrating that the ferroelectric polarization degenerates because of the thermal disturbance at high temperature [33]. In addition, the monotonic decreasing variation of polarization at $x = 0.15$ elucidating that a steady ECE performance as a function of temperature would be observed, that is to say, a flat ΔT – T curves would be presented in this composition [34].

The temperature dependence of ΔT values calculated according to Eq. (1) measured at different electric fields is given in Figs. 5(a)–5(d), in which $(\partial P/\partial T)_E$ is procured from the fourth-order polynomial fitting of the virgin P_{\max} – T curves [12]. It is clear that the enhanced ΔT values can be observed in the ceramics with $x = 0.08$ – 0.15 when the applied external electric field increases due to the optimal ordered state under the high electric fields [35]. In addition, the ECE peak gradually shifts to a lower temperature when x increases from 0.08 to 0.15 , well matching the decreased T_C values with increased x

content (Fig. 3). Under the applied external electric fields of 40 kV/cm, the maximum ΔT value of 0.61 , 0.59 , 0.64 , and 0.25 K are, respectively, obtained in $x = 0.08$, 0.11 , 0.13 , and 0.15 [Fig. 5(e)]. Furthermore, the electrocaloric coefficient ($\Delta T/\Delta E$) is also a critical argument for practical applications. Figure 5(f) presents the composition-dependent $\Delta T/\Delta E$ values measured at 40 kV/cm. The largest $\Delta T/\Delta E$ value of 0.16 K mm/kV is attained at $x = 0.13$. Generally, Maxwell’s relation can be strictly used in bulk monodomain single crystals only, while only a qualitative agreement could be expected for multidomain ferroelectric and nonergodic materials. Thus, the direct measurement of ECE must be carried out to confirm the availability of the calculated ΔT results using the indirect method [22]. Figure 5(g) displays the heat flow consequences obtained by using the modified DSC instrument to validate the fulfilling indirect ECE properties of the ceramics with $x = 0.13$. It is noted that the applied external electric fields could produce an uphill exothermic peak, while a decurrent endothermic peak is observed when the electric fields withdraw from the samples [14]. It can be seen that both the exothermic and endothermic peaks increase with the aggrandized applied electric fields, and presenting a reversible ECE and an increased ΔT

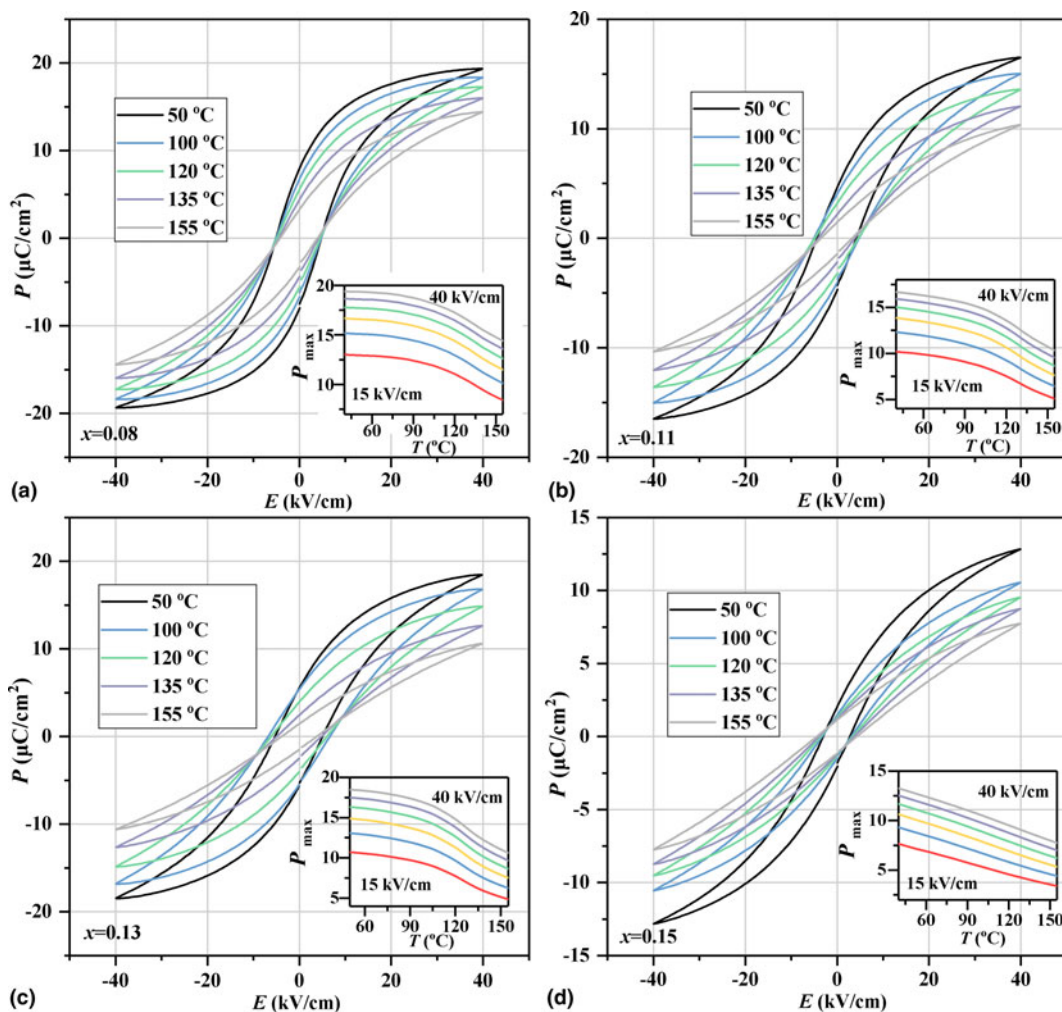


Figure 4: Temperature-dependent P - E loops of (a) $x = 0.08$, (b) $x = 0.11$, (c) $x = 0.13$, and (d) $x = 0.15$, the insert picture showing the temperature dependence of P_{\max} measured at different electric fields.

value with the increased electric fields as well, as shown in Figs. 5(g) and 5(h). Actually, the direct ΔT values could be calculated using the formula of

$$\Delta T = \frac{\Delta Q}{C_p}, \quad (5)$$

where ΔQ is the heat exchange values calculated using the area of the endothermic peaks under different electric fields [4, 36]. As shown in Fig. 5(h), although a slightly disparate ΔT is attained between the direct and indirect methods, the similar result of ΔT attained from those two methods indicates that the result calculated from the indirect method is in receivable. Besides, the discrepancy between the direct and indirect results might be ascribed to the existed extra contribution which is not considered in the Maxwell's relations. And the contribution could be relevant to dynamically PNRs and diffused FP phase transition in the vicinity of T_m , which offer extra entropy change under external electric fields [37].

According to Eq. (2), the applied external electric fields also have a vital role in ECE performance of the ceramics. And out of the consideration of the enhanced ΔT value under the higher electric field, a high electric field of 65 kV/cm is applied to the ceramics with $x = 0.13$. As shown in Fig. 6(a), typical P - E loops are obtained at different temperatures. And the extracted P_{\max} values from Fig. 6(a) decrease with the elevated temperature at diverse electric fields, as shown in Fig. 6(b). The calculated ΔT and $\Delta T/\Delta E$ values measured at different electric fields present a similar trend, both increasing first and then decreasing as the temperature goes up. And the maximum ΔT and $\Delta T/\Delta E$ of 1.24 K and 0.19 K mm/kV are found at the maximum electric field of 65 kV/cm, as plotted in Figs. 6(c) and 6(d), respectively. The ΔT value is almost doubled when the external applied electric field elevated from 40 to 65 kV/cm, proving the significant contribution of electric field to ECE performance.

Figure 7(a) shows the comparison of ΔT values as a function of electric fields of this work and other KNN-based

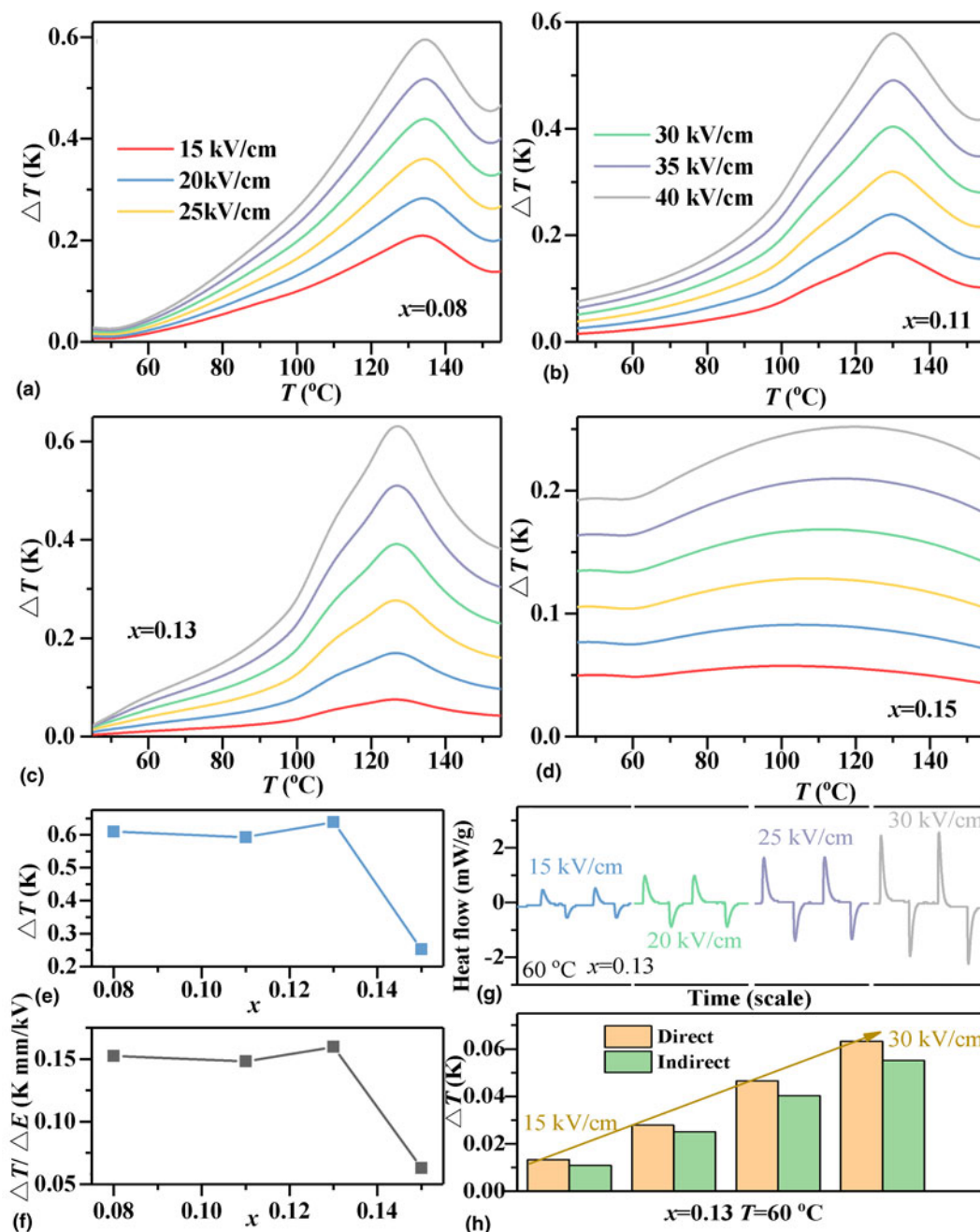


Figure 5: ΔT - T curves under different electric fields of the ceramics with (a) $x=0.08$, (b) $x=0.11$, (c) $x=0.13$, and (d) $x=0.15$; Composition-dependent (e) ΔT and (f) $\Delta T/\Delta E$ of the ceramics; (g) DSC heat flow curve of the ceramics with $x=0.13$ measured at 60°C under different DC electric fields utilizing the direct measurement; (h) A composition of ΔT values obtaining from direct and indirect measurements at 60°C for the ceramics with $x=0.13$.

ceramics with FF or FP transitions [12, 13, 14, 34, 38, 39, 40, 41]. It can be seen that the ΔT values of this work exceed most of the other KNN-based ceramics under the same or higher electric fields, illustrating that the ceramics prepared in this work are hopeful materials for practical refrigeration applications. Apart from the ΔT values, the temperature span is also a crucial parameter for practical applications. Figure 7 (b) shows the comparison of temperature span for the ceramics with different ΔT values. For the lower $\Delta T \geq 0.2$ K, the $x=0.15$

sample presents the largest temperature span of 90°C , which could be ascribed to the temperature region above T_C ($T_C \sim 60^{\circ}\text{C}$), but unfortunately together with a rapid deterioration ΔT value [Fig. 5(e)]. For the $x=0.08$, 0.11 , and 0.13 ceramics with similar ΔT , similar temperature span could be attained as well. Furthermore, it is noted that for the ECE benchmark of $\Delta T \geq 0.4$ K and $\Delta T \geq 0.5$ K, the beginning temperature of the temperature span of the ceramic with $x=0.13$ is lower than the ceramics with $x=0.08$ and 0.11 , which is benefit

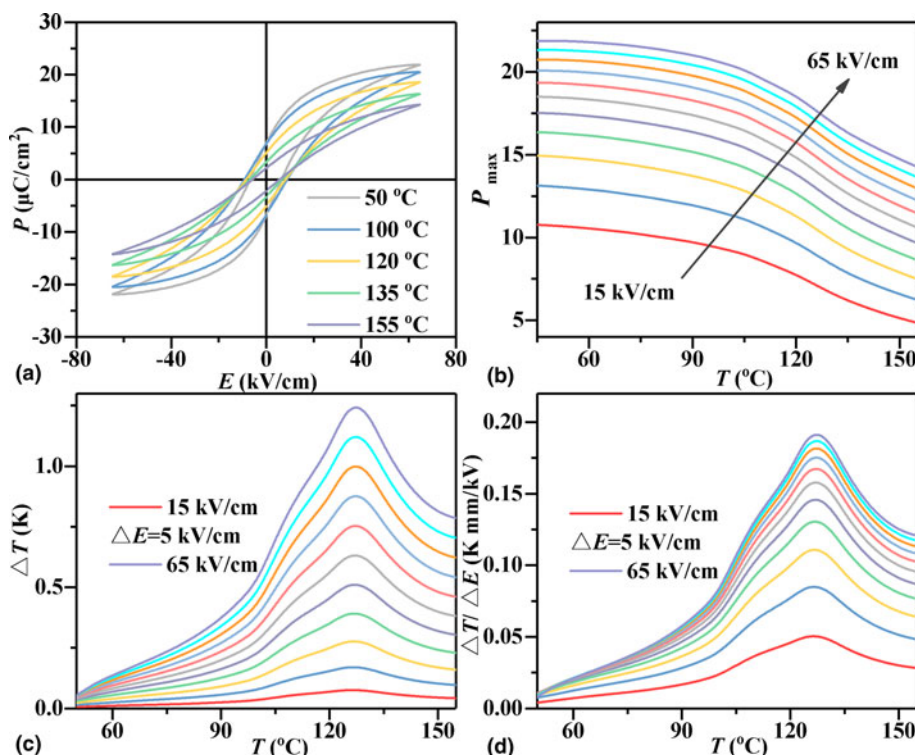


Figure 6: Temperature-dependent (a) P - E curves measured at 65 kV/cm and (b) P_{max} values measured at different electric fields. (c) ΔT and (d) $\Delta T/\Delta E$ values measured at different electric fields of the ceramics with $x = 0.13$.

from the decreased T_C value compared to 0.08 and 0.11 compositions [Fig. 2(a)]. In addition, it is noted that the elevated electric fields could improve the ΔT and temperature span simultaneously, confirming the significance of the high electric fields (or breakdown strength) for obtaining high ECE performance neglecting the effects of phase transition. Figure 7(c) shows the comparison of temperature span at different ECE benchmark among this work and other KNN-based lead-free ceramics. It is shown that the temperature span measured at 40 kV/cm is comparable to other KNN-based ceramics. And there is a large jump of temperature span by applying a higher electric field, especially for the region of $\Delta T \geq 0.5$ K. Piezoresponse force microscopic (PFM) amplitude and phase images are conducted to further investigate the domain configurations of the ceramics, which could affect the ferroelectric properties of the ceramics and finally influence the ECE performance as well, as shown in Figs. 7(d)–7(f). A micro positive tip voltage is used to characterize the domain configuration, which rarely undermine the surface structure of the ceramics. As a consequence, the PFM amplitude and phase images we attained could be seen as the virgin domain structure of the ceramics. As reported, the long-range-ordered ferroelectric domains would be broken due to the chemical modification, and polar nanoregions are existed in the nonpolar matrix (pseudo-cubic phase structure) in the high chemical substitution content [18]. Inhomogeneous nano-sized domains could be observed in the ceramics with $x = 0.11$ –0.15, which is a

typical phenomenon of relaxor ferroelectric [42]. In addition, it can be seen that the proportion of nanodomains increases a little in the first and then decreases with the increased x from 0.11 to 0.15.

As expected, shifting the FP phase transition toward room temperature together with inducing diffused phase transition is beneficial for ECE performance, which improves the ΔT values and temperature span to some extent. According to the macro ferroelectric and dielectric properties as well as microstructure of the ceramics, the phase structure and domain configuration are contributed to the magnitude of ΔT values. And the underlying mechanism of ECE performance in this work is presented in Fig. 8. The high diffuse degree γ of 1.6–1.95 and the diffused FP phase transition in the ceramics with $x = 0.08$ –0.15 illustrate a distinct relaxor characteristic, and the increasing volume fraction of PNRs could be observed around T_C [43], as shown in Figs. 2 and 8. In general, almost all the nanodomains and the entire PNRs could switch back to their original direction after removing the external electric fields in relaxor ferroelectrics [43]. The slightly increased amount of nanodomains in $x = 0.13$ compared to $x = 0.11$ leads to the slight difference entropy change, corresponding to the small diverse in P_{max} in Fig. 4. But the difference we mentioned above among the ceramics with $x = 0.08$ –0.13 is faint, so a relatively large entropy change is exhibited in the ceramics with $x = 0.08$ –0.13. In contrast, the ceramic with $x = 0.15$ with the largest diffuseness value presents a slimmer P - E loop with smaller P_{max} due to the decreased

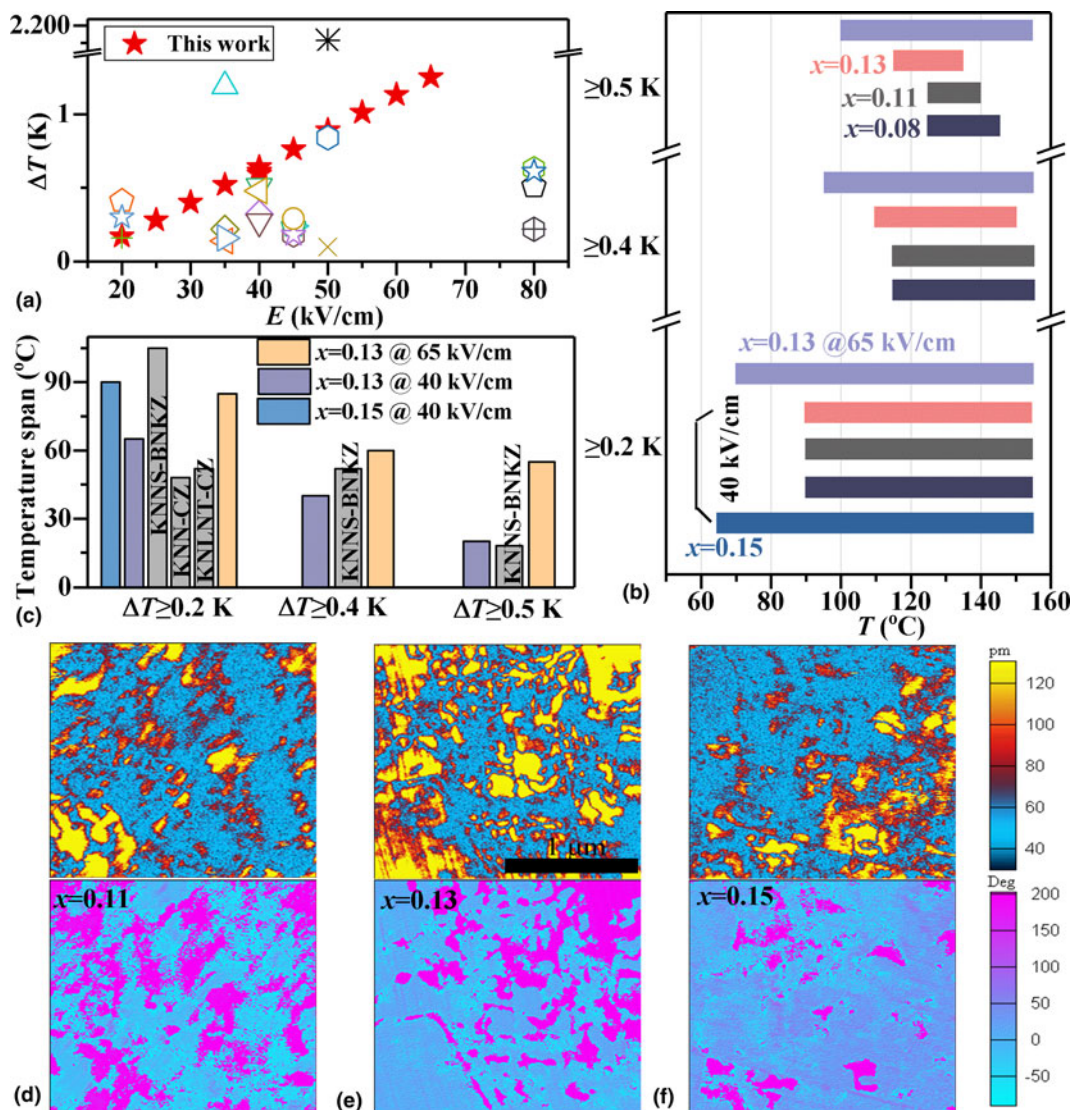


Figure 7: (a) Comparison of ΔT values of this work (the red star) and other KNN-based ceramics under different electric fields [12, 13, 14, 34, 38, 39, 40, 41]; (b) Distribution of temperature span of different ΔT values; (c) Comparison of the temperature span of ΔT values among this work and other KNN-based ceramics (at 40 kV/cm) [12, 14, 40]; Out-of-plane PFM amplitude and phase images of (d) $x = 0.11$, (e) $x = 0.13$, and (f) $x = 0.15$ ceramics.

amount of nanodomains and the increased amount of PNRs at around FP transition close to room temperature, finally leading to the rapidly decreased entropy change value as well. As a result, the large ΔT obtained in the ceramics with $x = 0.08 - 0.13$ is mainly attributed to the large P_{\max} values and large ΔP changes when the ceramics undergo the FP phase transition as the environmental temperature rising.

Conclusions

In this work, a diffused FP phase transition, which is close to room temperature, is constructed by suitable composition modification. Large ECE performance ($\Delta T = 1.24$ K and $\Delta T/\Delta E = 0.19$ K mm/kV) is observed under the electric field of 65 kV/cm. And a good temperature span of 55 °C at

the ECE benchmark of $\Delta T \geq 0.5$ K could also be obtained. The ECE results have been confirmed by the indirect and direct measurements. Besides, this work opens a new view of designing high-performance ceramics for refrigeration applications.

Experimental Procedure

Lead-free $0.97(\text{Na}_{0.5}\text{K}_{0.5})(\text{Nb}_{1-x}\text{Sb}_x)\text{NbO}_3 - 0.03\text{CaZrO}_3 - 1.0\%$ mol CuO (abbreviated as $\text{KNNS}_x\text{-CZ-CuO}$) samples were prepared by the conventional solid-state method. K_2CO_3 (99%), Na_2CO_3 (99.8%), Nb_2O_5 (99.95%), Sb_2O_3 (99.99%), CaCO_3 , and CuO were weighed and milled with ethanol for 24 h. After drying the mixture, the mixed powders were calcined at

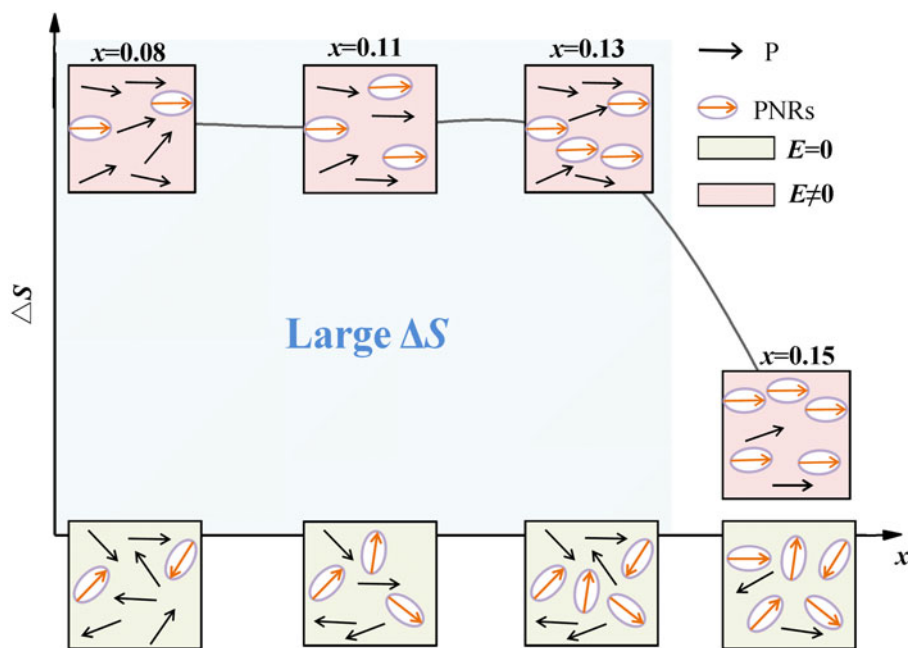


Figure 8: Schematic of entropy change as a function of x based on the domain structure.

850 °C for 6 h. Subsequently, the calcined powders were remilled with 1.0% mol CuO for 24 h and then dried. After that, the dried powders were pressed into disc-shaped pellets of 10 mm in diameter under a pressure of 10 MPa using 8% PVA as binder. The pellets were sintered at 1060–1080 °C for 3 h after removing the binder at 850 °C for 2 h. Both surfaces of the sintered samples were polished and then coated with silver for measuring the electric and ferroelectric behavior. Then, the samples were poled at room temperature under a DC field of 40 kV/cm for 20 min.

The phase structure of the ceramic samples was characterized by XRD (Bruker D8 Advanced XRD, Bruker AXS Inc., Madison, WI; Cu K_{α}). The polarization–electric field (P – E) hysteresis loops were obtained utilizing TF-2000 at a fixed frequency of 5 Hz. The temperature-dependent ϵ_r was measured using an LCR analyzer (HP 4980, Agilent, USA). Direct measurements of ECE were conducted using a modified DSC (Q2000, TA Instruments, New Castle, DE), and a DC power supplier (ET2671A, ENTAI, China) was utilized to apply external electric fields on the ceramics. PFM (Asylum Research, MFP-3D) with a conductive Pt–Ir-coated tips (Nanosensors, Neuchatel, Switzerland) was used to gather the domain patterns. The out-of-plane piezoresponse of domains was obtained utilizing the AC tiny tip voltage of 2 V among the area of $2 \times 2 \mu\text{m}^2$.

Acknowledgments

The authors gratefully acknowledge the supports of the National Science Foundation of China (NSFC No. 51722208).

References

1. G. Zhang, Z. Chen, B. Fan, J. Liu, M. Chen, M. Shen, P. Liu, Y. Zeng, S. Jiang, and Q. Wang: Large enhancement of the electrocaloric effect in PLZT ceramics prepared by hot-pressing. *APL Mater.* **4**, 064103 (2016).
2. S. Fähler and V.K. Pecharsky: Caloric effects in ferroic materials. *MRS Bull.* **43**, 264 (2018).
3. J. J. Wang, D. Fortino, B. Wang, X. Zhao, and L.Q. Chen: Extraordinarily large electrocaloric strength of metal-free perovskites. *Adv. Mater.* **32**, 1906224 (2020).
4. X. Moya, S.K. Narayan, and N.D. Mathur: Caloric materials near ferroic phase transitions. *Nat. Mater.* **13**, 439 (2014).
5. A. Mischenko, Q. Zhang, J.F. Scott, R.W. Whatmore, and N.D. Mathur: Giant electrocaloric effect in thin-film $\text{PbZr}_{0.95}\text{Ti}_{0.05}\text{O}_3$. *Science* **311**, 1270 (2006).
6. Y. Yu, F. Gao, F. Weyland, H. Du, L. Jin, L. Hou, Z. Yang, N. Novak, and S. Qu: Significantly enhanced room temperature electrocaloric response with superior thermal stability in sodium niobate-based bulk ceramics. *J. Mater. Chem. A* **7**, 11665 (2019).
7. J. Koruza, B. Roži, G. Cordoyiannis, B. Malič, and Z. Kutnjak: Large electrocaloric effect in lead-free $\text{K}_{0.5}\text{Na}_{0.5}\text{NbO}_3$ - SrTiO_3 ceramics. *Appl. Phys. Lett.* **106**, 202905 (2015).
8. C. Zhao, Y. Huang, and J. Wu: Multifunctional barium titanate ceramics via chemical modification tuning phase structure. *InfoMat* (2020). doi:10.1002/inf2.12147.
9. R. Zuo and J. Fu: Rhombohedral-tetragonal phase coexistence and piezoelectric properties of $(\text{NaK})(\text{NbSb})\text{O}_3$ - LiTaO_3 - BaZrO_3 lead-free ceramics. *J. Am. Ceram. Soc.* **94**, 1467 (2011).

10. H. Tao, H. Wu, Y. Liu, Y. Zhang, J. Wu, F. Li, X. Lyu, C. Zhao, D. Xiao, J. Zhu, and S.J. Pennycook: Ultrahigh performance in lead-free piezoceramics utilizing a relaxor slush polar state with multiphase coexistence. *J. Am. Chem. Soc.* **141**, 13987 (2019).
11. L. Zhao, X. Ke, Z. Zhou, X. Liao, J. Li, Y. Wang, M. Wu, T. Li, Y. Bai, and X. Ren: Large electrocaloric effect over a wide temperature range in BaTiO₃-modified lead-free ceramics. *J. Mater. Chem. C* **7**, 1353 (2019).
12. X. Wang, J. Wu, B. Dkhil, B. Xu, X. Wang, G. Dong, G. Yang, and X. Lou: Enhanced electrocaloric effect near polymorphic phase boundary in lead-free potassium sodium niobate ceramics. *Appl. Phys. Lett.* **110**, 063904 (2017).
13. R. Kumar and S. Singh: Enhanced electrocaloric response and high energy-storage properties in lead-free (1-x)(K_{0.5}Na_{0.5})NbO₃-xSrZrO₃ nanocrystalline ceramics. *J. Alloys Compd.* **764**, 289 (2018).
14. J. Yang, Y. Zhao, X. Lou, J. Wu, and X. Hao: Synergistically optimizing electrocaloric effects and temperature span in KNN-based ceramics utilizing a relaxor multiphase boundary. *J. Mater. Chem. C* **8**, 4030 (2020).
15. J. Wu, D. Xiao, and J. Zhu: Potassium-sodium niobate lead-free piezoelectric materials: Past, present, and future of phase boundaries. *Chem. Rev.* **115**, 2559 (2015).
16. Y. Li, Y. Zhen, W. Wang, Z. Fang, Z. Jia, J. Zhang, H. Zhong, J. Wu, Y. Yan, Q. Xue, and F. Zhu: Enhanced energy storage density and discharge efficiency in potassium sodium niobate-based ceramics prepared using a new scheme. *J. Eur. Ceram. Soc.* **40**, 2357 (2020).
17. X. Lv and J. Wu: Effects of a phase engineering strategy on the strain properties in KNN-based ceramics. *J. Mater. Chem. C* **7**, 2037 (2019).
18. B. Wu, C. Zhao, Y. Huang, J. Yin, W. Wu, and J. Wu: Superior electrostrictive effect in relaxor potassium sodium niobate based ferroelectrics. *ACS Appl. Mater. Interfaces* **12**, 25050 (2020).
19. X. Li, S.G. Lu, X.Z. Chen, H. Gu, X. Qian, and Q.M. Zhang: Pyroelectric and electrocaloric materials. *J. Mater. Chem. C* **1**, 23 (2013).
20. G. Vats, A. Kumar, N. Ortega, C.R. Bowen, and R.S. Katiyar: Giant pyroelectric energy harvesting and a negative electrocaloric effect in multilayered nanostructures. *Energ. Environ. Sci.* **9**, 1335 (2016).
21. M. Guo, M. Wu, W. Gao, B. Sun, and X. Lou: Giant negative electrocaloric effect in antiferroelectric PbZrO₃ thin films in an ultra-low temperature range. *J. Mater. Chem. C* **7**, 617 (2019).
22. M. Valant: Electrocaloric materials for future solid-state refrigeration technologies. *Prog. Mater. Sci.* **57**, 980 (2012).
23. C. Zhao, J. Yang, Y. Huang, X. Hao, and J. Wu: Broad-temperature-span and large electrocaloric effect in lead-free ceramics utilizing successive and metastable phase transitions. *J. Mater. Chem. A* **7**, 25526 (2019).
24. E. Li, H. Kakemoto, S. Wada, and T. Tsurumi: Influence of CuO on the structure and piezoelectric properties of the alkaline niobate-based lead-free ceramics. *J. Am. Ceram. Soc.* **90**, 1787 (2007).
25. J.B. Lim, S. Zhang, J.H. Jeon, and T.R. Shrout: (K,Na)NbO₃-based ceramics for piezoelectric “hard” lead-free materials. *J. Am. Ceram. Soc.* **93**, 1218 (2010).
26. H.Y. Park, J.Y. Choi, M.K. Choi, K.H. Cho, S. Nahm, H.G. Lee, and H.W. Kang: Effect of CuO on the sintering temperature and piezoelectric properties of (Na_{0.5}K_{0.5})NbO₃ lead-free piezoelectric ceramics. *J. Am. Ceram. Soc.* **91**, 2374 (2008).
27. Y. Chang, S.F. Poterala, Z. Yang, S.T. McKinstry, and G.L. Messing: Microstructure development and piezoelectric properties of highly textured CuO-doped KNN by templated grain growth. *J. Mater. Res.* **25**, 687 (2011).
28. R.D. Shannon: Revised effective ionic radii and systematic studies of interatomic distances in halides and chalcogenides. *Acta Cryst.* **A32**, 751 (1976).
29. X. Lv, J. Zhu, D. Xiao, X. Zhang, and J. Wu: Emerging new phase boundary in potassium sodium-niobate based ceramics. *Chem. Soc. Rev.* **49**, 671 (2020).
30. Y. Huang, C. Zhao, J. Yin, X. Lv, J. Ma, and J. Wu: Giant electrostrictive effect in lead-free barium titanate-based ceramics via A-site ion-pairs engineering. *J. Mater. Chem. A* **7**, 17366 (2019).
31. J. Xing, S. Xie, B. Wu, Z. Tan, L. Jiang, L. Xie, Y. Cheng, J. Wu, D. Xiao, and J. Zhu: Influence of different lanthanide ions on the structure and properties of potassium sodium niobate based ceramics. *Scr. Mater.* **177**, 186 (2020).
32. X. Ren, Z. Peng, B. Chen, Q. Shi, X. Qiao, D. Wu, G. Li, L. Jin, Z. Yang, and X. Chao: A compromise between piezoelectricity and transparency in KNN-based ceramics: The dual functions of Li₂O addition. *J. Eur. Ceram. Soc.* **40**, 2331 (2020).
33. F. Huang, H. Tian, X. Meng, P. Tan, X. Cao, Y. Bai, C. Hu, and Z. Zhou: Large room temperature electrocaloric effect in KTa_{1-x}Nb_xO₃ single crystal. *Phys. Status Solidi RRL* **13**, 1800515 (2019).
34. J. Li, Y. Bai, S. Qin, J. Fu, R. Zuo, and L. Qiao: Direct and indirect characterization of electrocaloric effect in (Na,K)NbO₃ based lead-free ceramics. *Appl. Phys. Lett.* **109**, 162902 (2016).
35. L. Zhang, C. Zhao, T. Zheng, and J. Wu: Large electrocaloric effect in (Bi_{0.5}Na_{0.5})TiO₃-based relaxor ferroelectrics. *ACS Appl. Mater. Interfaces* **12**, 33934 (2020).
36. F.L. Goupil, A.K. Axelsson, L.J. Dunne, M. Valant, G. Manos, T. Lukasiewicz, J. Dec, A. Berenov, and N.M. Alford: Anisotropy of the electrocaloric effect in lead-free relaxor ferroelectrics. *Adv. Energ. Mater.* **4**, 1301688 (2014).

37. **M. Sanlialp, V.V. Shvartsman, M. Acosta, B. Dkhil, and D.C. Lupascu:** Strong electrocaloric effect in lead-free 0.65Ba (Zr_{0.2}Ti_{0.8})O₃-0.35(Ba_{0.7}Ca_{0.3})TiO₃ ceramics obtained by direct measurements. *Appl. Phys. Lett.* **106**, 062901 (2015).
38. **R. Kumar, A. Kumar, and S. Singh:** Large electrocaloric response and energy storage study in environmentally friendly (1-x) K_{0.5}Na_{0.5}NbO₃-xLaNbO₃ nanocrystalline ceramics. *Sustain. Energ. Fuels* **2**, 2698 (2018).
39. **R. Kumar, A. Kumar, and S. Singh:** Coexistence of large negative and positive electrocaloric effects and energy storage performance in LiNbO₃ doped K_{0.5}Na_{0.5}NbO₃ nanocrystalline ceramics. *ACS App. Electron. Mater.* **1**, 454 (2019).
40. **S. Kumar and S. Singh:** Study of electrocaloric effect in lead-free 0.9K_{0.5}Na_{0.5}NbO₃-0.1CaZrO₃ solid solution ceramics. *J. Mater. Sci.: Mater. Electron.* **30**, 12924 (2019).
41. **J. Yang and X. Hao:** Electrocaloric effect and pyroelectric performance in (K,Na)NbO₃-based lead-free ceramics. *J. Am. Ceram. Soc.* **102**, 6817 (2019).
42. **S.M. Pilgrim, A.E. Sutherland, and S.R. Winzer:** Diffuseness as a useful parameter for relaxor ceramics. *J. Am. Ceram. Soc.* **73**, 3122 (1990).
43. **Y. Huang, C. Zhao, B. Wu, and J. Wu:** Multifunctional BaTiO₃-based relaxor ferroelectrics toward excellent energy storage performance and electrostrictive strain benefiting from crossover region. *ACS Appl. Mater. Interfaces* **12**, 23885 (2020).